Analysis of the internal heat losses in a thermoelectric generator

CrossMark

R. Bjørk[*], D.V. Christensen, D. Eriksen, N. Pryds

Department of Energy Conversion and Storage, Technical University of Denmark – DTU, Frederiksborgvej 399, DK-4000 Roskilde, Denmark

ABSTRACT

A 3D thermoelectric numerical model is used to investigate different internal heat loss mechanisms for a thermoelectric generator with bismuth telluride p- and n-legs. The model considers all thermoelectric effects, temperature dependent material parameters and simultaneous convective, conductive and radiative heat losses, including surface to surface radiation. For radiative heat losses it is shown that for the temperatures considered here, surface to ambient radiation is a good approximation of the heat loss. For conductive heat transfer the module efficiency is shown to be comparable to the case of radiative losses. Finally, heat losses due to internal natural convection in the module is shown to be negligible for the millimetre sized modules considered here. The combined case of radiative and conductive heat transfer resulted in the lowest efficiency. The optimized load resistance is found to decrease for increased heat loss. The leg dimensions are varied for all heat losses cases and it is shown that the ideal way to construct a TEG module with minimal heat losses and maximum efficiency is to either use a good insulating material between the legs or evacuate the module completely, and use small and wide legs closely spaced.

© 2014 Elsevier Masson SAS. All rights reserved.

1. Introduction

Power generation through the thermoelectric effect is a subject of increasing interest both scientifically and commercially. The performance of a thermoelectric generator (TEG) is often estimated using numerical modelling before actual physical modules are constructed. This allows for the development of new and better thermoelectric generators in a cost effective manner, as well as for designing and optimizing modules to achieve as high an efficiency as possible. To accurately design the most efficient module possible, a large number of factors must be taken into account including geometric parameters, temperature dependence of the material properties, heat losses and thermal and electrical contact resistances.

A substantial number of numerical models of thermoelectric generators, both of unicouples and modules, have been published, but most of these only consider the ideal case with no heat losses and contact resistances. While the latter effect presents some challenges to determine experimentally, it can easily be included in a numerical model, if the contact resistance is known from experimental measurements. Including heat losses in a numerical model is more troublesome, but is never the less important as heat losses can significantly degrade the performance of a TEG. Experimental

thermoelectric generator output is known to deviate from a TEG model with no heat losses; for example have heat losses determined experimentally previously been reported to reduce the efficiency by about 40–50% [1,2].

Heat losses have been considered in numerical models of TEGs in both one, two and three dimensional models. Muto et al. [3] considered a 1D TEG model where the radiative heat loss is given by Stefan–Boltzmann law for a specified perimeter length, whereas Meng et al. [4] consider a 1D model including all heat losses (radiative, conductive and convective) by assuming the temperature in the air gap between the TEG legs to be equal to that in the legs themselves. For three dimensions a substantial number of publications exists where a TEG is modelled, however without heat losses, using a finite element model (FEM) [5–11]. When heat losses are considered, most frequently the models reported in literature only consider a single heat loss mechanism and typically the heat loss mechanisms are simplified substantially. For general heat loss and for fluid flow problems often only heat loss through a simple heat transfer coefficient has been considered [12–17]. For heat loss through radiation, only surface to ambient radiation and not surface to surface radiation has been considered [14,16,18,19]. Using the simplified physical assumptions presented above, different heat loss mechanisms have been compared, where it was found that the convectional losses are greatest followed by radiation and thermal conduction of a solid filling material within the voids of the module [19].

* Corresponding author.
  E-mail address: rabj@dtu.dk (R. Bjørk).

Here we consider the performance of a TEG, accounting for heat losses in full detail numerically by modelling surface to surface radiation as well as conductive and convective heat losses, where the flow field is completely modelled for the latter. For each heat loss mechanism the influence of both geometrical factors and physical parameters are investigated, with the aim of determining the influence of the various heat loss mechanisms on the performance of a TEG. This knowledge will allow for the optimal TEG with regards to cost and efficiency to be designed.

2. Three dimensional TEG model

A 3D thermoelectric model of a module with p- and n-type legs, electrodes and substrates has been set up and implemented in the commercial finite element software Comsol Multiphysics [20]. The coupled differential equations describe the electrical current density, $\mathbf{J}$, and the heat flux, $\mathbf{J}_Q$, as [21]

$$-\mathbf{J} = \sigma\nabla V + \sigma\alpha\nabla T \\ \mathbf{J}_Q = -\kappa\nabla T + T\alpha\mathbf{J} \tag{1}$$

Here σ is the electrical conductivity, V is the electrical potential, α is the Seebeck coefficient, T is the temperature, and κ is the thermal conductivity. In the equation for $\mathbf{J}$, the first term is Ohms law, while the second describes the Seebeck effect. In the equation for $\mathbf{J}_Q$ the first term describes Fourier heat conduction, while the latter describes the Peltier effect. Numerically, the latter term in the equation for $\mathbf{J}$ is implemented as an "External Current Density" in Comsol, while the expression for $\mathbf{J}_Q$ is modified through a "Weak Expression" [29].

In steady state operation the current density is divergence-free

$$\nabla\cdot\mathbf{J} = 0, \tag{2}$$

whereas the heat flux is given by

$$\nabla\cdot\mathbf{J}_Q = -\nabla\cdot(V\mathbf{J}). \tag{3}$$

For the case of steady state operation, the energy accumulation, $\dot{e}$, must be zero, i.e.

$$\dot{e} = \nabla\cdot(\kappa\nabla T) - \nabla\cdot((V + T\alpha)\mathbf{J}) = 0. \tag{4}$$

Remembering that the current is divergence-free the energy accumulation becomes

$$\dot{e} = \nabla\cdot(\kappa\nabla T) - \mathbf{J}\cdot\left(\sigma^{-1}\mathbf{J}\right) - T\nabla\alpha\cdot\mathbf{J}. \tag{5}$$

where the middle term is the Joule heating and the latter term is the Thomson effect, both of which are present in the simulations.

These equations are solved on a finite element mesh for the desired geometry and thermal and electrical boundary conditions. The geometry considered here is that of several unicouples connected electrically in serial and thermally in parallel into a module. Either the material properties of the electrodes must be specified or an infinitely good electrical contact can be assumed. An external electrical load resistance, R_{ext}, is applied to the TEG. This is modelled as a boundary condition, described as a thin sheet of resistive material, with conductivity σ_s and thickness d_s, connected to a reference potential $V_{ref} = 0$ in one end of the module. The equation for this boundary condition is

$$\mathbf{n}\cdot(\mathbf{J}_1 - \mathbf{J}_2) = \frac{\sigma_s}{d_s}\left(V - V_{ref}\right), \tag{6}$$

where $\mathbf{n}$ is the normal vector to the surface. The other end of the module is assumed connected to ground, $V = 0$. All surfaces of the

TE legs not exposed to the electrodes are assumed to be electrically insulating, i.e. $\mathbf{J}\cdot\mathbf{n} = 0$, while the current is conserved over all internal boundaries. Finally, a contact resistance can be specified on all boundaries, in order to model an imperfect joining between the legs and the electrodes. However, here we assume the joining to be perfect in all cases.

Thermally, any two parameters out of the hot side temperature, cold side temperature, hot side heat flux and cold side heat flux must be specified as input parameters to the model. The thermal boundary conditions depend on the heat losses modelled, e.g. whether an infinite module or a module of finite size, with heat loss through the sides of the module, is considered. Here, we consider modules where no heat is lost through the sides of the module, but only lost internally in the module.

2.1. Radiative heat losses

If radiative heat losses are considered, for a surface radiating through a transparent medium, the radiative heat flux is given by the difference between the incoming radiation and the radiation leaving the surface, i.e.

$$Q = \varepsilon\left(G - \sigma_{SB}T^4\right) \tag{7}$$

where ε is the emissivity, G is the incoming radiative heat flux, or irradiation, and $\sigma_{SB} = 5.67 * 10^8$ W m^{-2} K^{-4} is Stefan–Boltzmanns constant. The irradiation can in general be written as

$$G = G_m + F_{amb}\sigma_{SB}T_{amb}^4 \tag{8}$$

where G_m is the mutual irradiation from other surfaces, F_{amb} is the ambient view factor, i.e. the fraction of the field of view that is not covered by other surfaces, and T_{amb} is the ambient temperature. The mutual irradiation will depend on the total outgoing radiative flux, or radiosity, J, at every other point in view. This results in an implicit equation for the radiosity as

$$J = (1 - \varepsilon)\left(G_m(J) + F_{amb}\sigma_{SB}T_{amb}^4\right) + \varepsilon\sigma_{SB}T^4 \tag{9}$$

where $G_m(J)$ is the mutual irradiation from other surfaces, which depends on J. For the case of blackbody radiation, the radiosity only depends on the temperature of the surface, as all incoming radiation is absorbed and converted to heat. These physics are built into and verified in the numerical software package Comsol used here [20]. The heat transfer equation and the equation for the radiosity are solved in parallel. When finding the view factor, shadow effects are taken into account. The view factor is evaluated using a z-buffered projection on the side of a hemicube to account for shadowing effects. This is somewhat analogue to rendering digital images of the geometry in five different directions and counting the pixels in each mesh element to evaluate its view factor [20].

For radiative heat transfer the side walls of the module are assumed to be so-called diffuse mirrors. This is a common approximation of a surface that is well insulated on one side and for which convection effects can be neglected on the opposite (radiating) side. It resembles a mirror that absorbs all irradiation and then radiates it back in all directions in all points. The radiative heat flux from a diffuse mirror boundary is zero [20].

2.2. Conductive and convective heat losses

For conductive heat losses the heat loss equation solved is simply that of pure conductive heat transfer (Eq. (1) for $\mathbf{J}_Q$ with

J = 0). For convective heat losses the full compressible Navier–Stokes equation and the heat transfer equation are solved, i.e.

$$\nabla \cdot (\rho \mathbf{u}) = 0$$

$$\rho \mathbf{u} \cdot \nabla \mathbf{u} = -\nabla p + \nabla \cdot \left(\mu \left(\nabla \mathbf{u} + (\nabla \mathbf{u})^T \right) - \frac{2}{3} \mu (\nabla \cdot \mathbf{u}) \mathbf{I} \right) + \mathbf{F} \quad (10)$$

where ρ is the density, $\mathbf{u}$ is the velocity vector, p is the pressure, μ is the dynamic viscosity and the body force is given by $\mathbf{F} = \rho \mathbf{g}$. In this equation the T denotes the transpose. In practice the pressure difference inside the TEG module will be small, which does allow the incompressible Navier–Stokes equation to be used, as the convection is only caused by a change in density with respect to temperature and not with pressure.

2.3. Modelled system

We consider a thermoelectric system consisting of a p-type nanocrystalline bulk Bi$_2$SbTe$_3$ [22] and n-type Bi$_2$Te$_3$ heat-treated nanocompound [23], with temperature dependent experimentally measured properties. The materials represent some of the best performing bismuth telluride materials published to date. This choice of materials allows the computed results to be applicable for almost all commercial modules to date, as these consist of p- and n-type BiTe legs. In all simulations the hot side temperature is taken to be 523.15 K and the cold side to 293.15 K, as these represent realistic operating temperatures for the BiTe materials, if any degradation performance of the BiTe over time at the high temperature is disregarded. A physical top and bottom plate is present in all simulations, with properties as given in Table 1. In all models no contact resistance, neither electrically or thermally, is included. Also, for all models the electrical contacts between legs are assumed to be perfect. This means that the potential generated by one leg is directly applied to the next leg in the module. This removes the need to physically resolve and mesh the electrical contacts between the legs.

3. Model verification

Before considering heat losses, we first consider a system with no heat losses, in order to verify the model and to find the optimal geometry of the system used for analysing heat losses. We consider a system with a leg length of 1 mm and hot and cold side temperatures as given in Table 1. For a TEG with no thermal losses, the efficiency, η, is defined as

$$\eta = \frac{P}{Q_{in}} \quad (11)$$

where P is the power produced, and Q_{in} is the heat flowing into the TEG, i.e. the sum of the heat flowing into the p- and n-leg, respectively. The power is simply given by $P = IV$, where I is the current produced and V is the total electric potential over the entire TEG module. The power per unit area is defined as the power produced divided with the total cross sectional area of the legs, i.e. $A_n + A_p$.

For a system with a fixed temperature span, but without heat losses, the efficiency only depends on the area ratio between cross-sectional areas of the p- and n-legs, A_n/A_p, and the load resistance, R_{ext}. The efficiency and power per area as function of the area ratio are shown in Fig. 1 for the load resistance that results in the highest values. The optimum efficiency and power per area occur at an optimal area ratio of around $A_n/A_p = 0.75$ in both cases. However, there is little decrease in the performance when slightly increasing the area ratio. In the following heat loss analysis we will fix the area ratio to $A_n/A_p = 1$, at which the no-heat-loss efficiency is 9%, as this is the area ratio usually found in commercial modules.

As can be seen from Fig. 1 there is an excellent agreement between the model presented here and a 1D model of a TEG [24,25] for the case of no heat losses [26]. The 1D model reformulates the general equation for the efficiency of a TEG, allowing for simple integration to determine the thermoelectric state variables through a unicouple. For the area ratio of $A_n/A_p = 1$, a detailed investigation of the temperature profile in both legs reveals this to be close to linear, with variation less than 3.5 K when comparing the same position in the n- and p-leg. This means that ideally, when regarding heat losses, placing the legs very closely together does not result in a large leg-to-leg heat transfer.

4. Heat losses mechanisms

We will consider heat loss by radiation, conduction and convection, both singlehandedly and simultaneously, as these are the heat loss mechanisms for a TEG. As previously mentioned we consider legs with dimensions of $1 \times 1 \times 1$ mm^3, which is close to the optimal area ratio and to the dimensions used in commercial TEG modules [27]. We have not optimized the cross-sectional area ratio between n- and p-legs for the different heat loss cases, as we wish to compare the magnitude of the different heat loss mechanisms for identical TEGs. For all modelled systems the external load resistance that optimizes the efficiency for the given system is found.

We consider whole modules, consisting of $n \times n$-legs, equidistantly spaced and topped with a hot plate and with a cold bottom plate. In some cases the efficiency is the same regardless of the value of n, but if this is not the case we consider modules with 2×2 or 4×4 legs. Such a case could be surface to surface radiation,

Table 1
The general module parameters. The thermal conductivity of the plates is identical to Ag at room temperature.

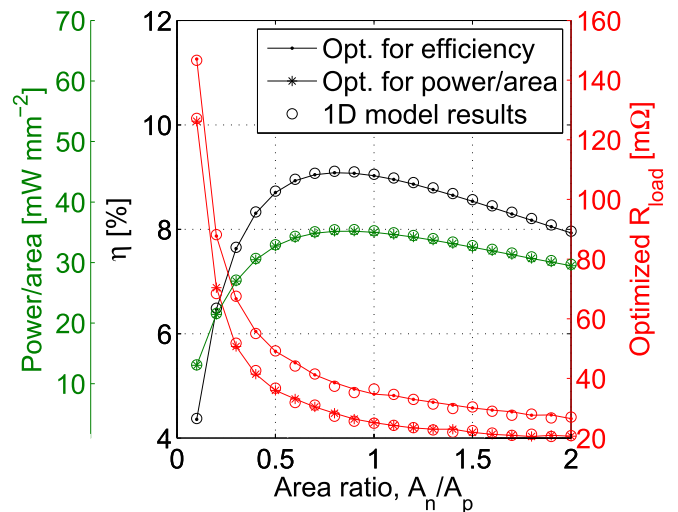| Module			
Legs and plates	$T_{hot} = 523.15$ K	$T_{cold} = 293.15$ K	$\varepsilon = 1$
	$x_{legs} = y_{legs} = z_{legs} = 1$ mm	$z_{plates} = 0.1$ mm	$\kappa_{plates} = 429$ W m^{-1} K^{-1}

Fig. 1. The optimized efficiency, η, and power per unit area and corresponding load resistances as function of area ratio. Also shown are results calculated using a 1D numerical model [24,25].

where the number of visible legs changes depending on the total number of legs. The legs are separated by a distance, termed the leg separation distance, and the top and bottom plates extend half of this distance out from the legs, as also shown in Fig. 2. In this way the area of the legs compared to the area of the plates does not vary based on the number of legs in the module.

The module has adiabatic side walls. Thus there is no external heat loss from the module, but only internal losses, e.g. heat passing directly from the hot plate to the cold plate, bypassing the legs. Modelling heat loss through the side walls would require knowing the conditions outside of the TEG, i.e. simulating the precise environment that the TEG is placed in, which would mean that the heat

losses could not be generally calculated. An illustration of a slice through the 3D system modelled is shown in Fig. 2, as well as some illustrations of the different heat transfer mechanisms considered.

For a module with heat losses, we will consider the system efficiency in the same way as for the no heat loss case, i.e. using Eq. (11), but where Q_{in} is taken as the total heat that is flowing from the hot side. This means that for e.g. a system in which the legs are embedded in a thermal insulator, the heat flowing directly from the hot side to the cold side through the thermal insulator, bypassing the legs completely, is included in the efficiency. Thus the efficiency measures the fraction of heat deducted from the hot side that is transformed into electricity by the TEG.
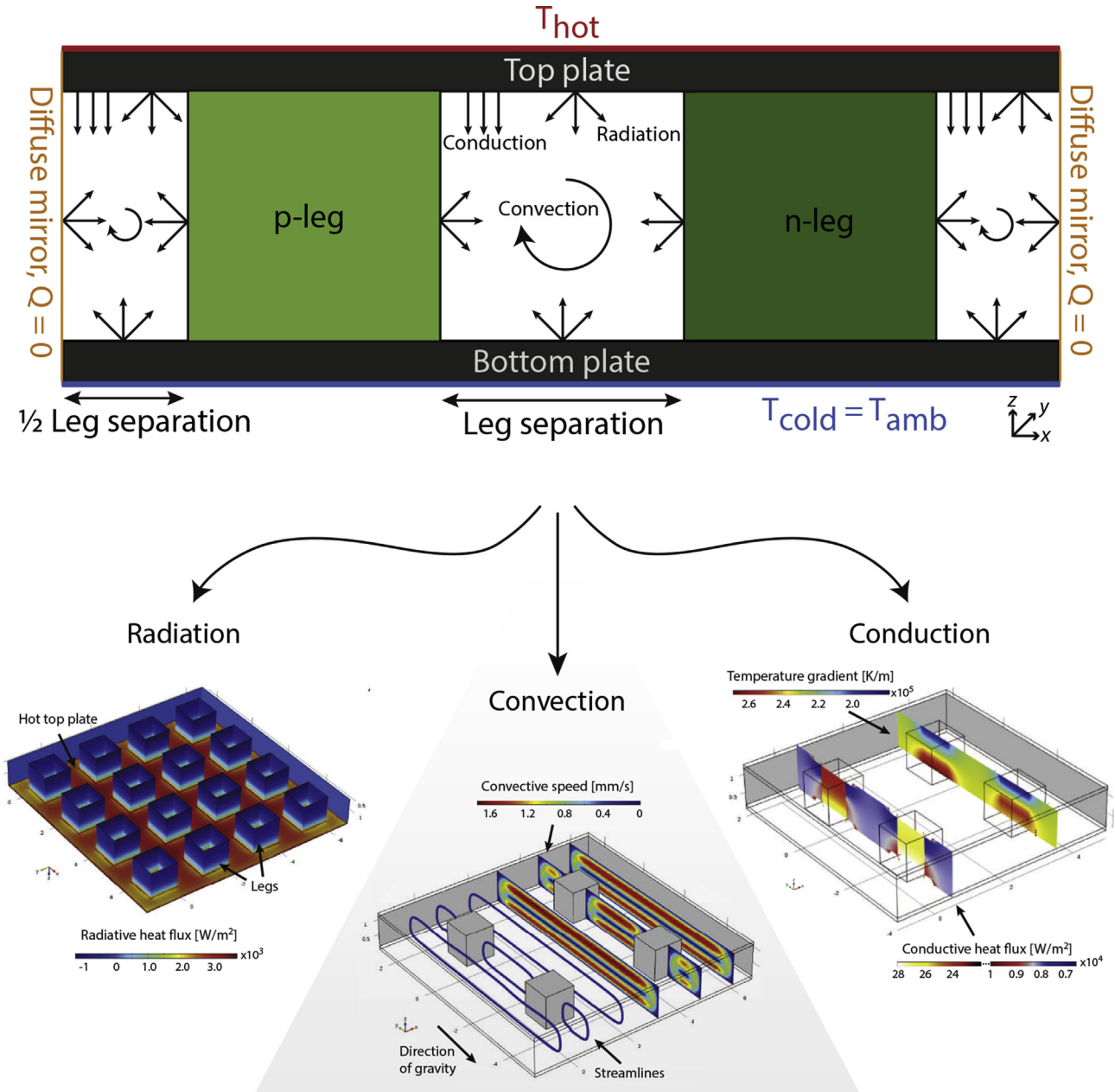

Fig. 2. An illustration of a slice of the thermoelectric system modelled for the different heat loss mechanisms considered. As previously mentioned the electrical connection between the legs is assumed to be perfect, removing the need to resolve the electrical contacts. The full 3D system is modelled. The distance between the legs is the same in the x and y directions. The different heat loss mechanisms modelled are also illustrated in the figure. The radiative heat flux for a 4×4 module including surface to surface radiation is shown for a leg separation distance of 1 mm, with the TEG viewed from the bottom. For the case of convection the flow field is shown for a 3 mm leg separation 2×2 module filled with air and including surface to surface radiation, conduction and convection. Finally the conductive heat flux and the temperature gradient is shown for the case of a 2 mm leg separation 2×2 module with a solid thermal insulator placed between the legs.

For each model containing different heat loss mechanisms a mesh size analysis was conducted to ensure that the results were not a function of mesh size. The normalized efficiency as function of mesh size is shown in Fig. 3, where the mesh used for the subsequent calculations have also been indicated.

5. Heat losses by conduction

We first consider the isolated case of heat losses only occurring by conduction. This corresponds to the situation where the legs in a TEG are surrounded by a thermally insulating material with a given thermal conductivity, κ, and an infinite electrical resistivity. We assume that no heat is lost through the outer sides of the module. As the temperature profiles in the n- and p-legs are almost identical in the no heat loss case, and as the legs have the same size, the efficiency is the same regardless of both the number of legs and the absolute size of the module.

The parameters varied for this system were leg separation values of 0.25−4 mm in steps of 0.25 mm and $\kappa = 10^x$ W m^{-1} K^{-1} from $x = -3$ to 0 in steps of 0.5. Shown in Fig. 4 is a surface plot of the efficiency as function of the leg separation distance and the thermal conductivity of the insulator material. The efficiency decreases for both increasing thermal conductivity and leg separation. This is expected as higher thermal conductivities and leg separations reduce the thermal resistance of the insulator material and thus increases the heat flux that bypasses the legs. Note that the thermal conductivity of the p- and n-leg materials is around 1 W m^{-1} K^{-1} for the materials considered here. For the thermal conductivity of still air, $\kappa \approx 0.02 - 0.04$ W m^{-1} K^{-1} for the temperature range considered here [28], the efficiency is 8−9% for small leg separations. Fig. 4 can be used to determine the optimal insulator material if e.g. there is a significant price difference between two insulator material, and the cost per efficiency loss ratio is known.

6. Heat losses by radiation

We next consider the case of heat loss by radiation only. In this configuration the sides of the module are modelled as diffuse mirrors, and the module is assumed completely evacuated. We consider modules of sizes 2 × 2 and 4 × 4, to evaluate the

Fig. 4. A surface plot of the efficiency, η, as function of the leg separation distance and the thermal conductivity of the insulator material. The efficiency is independent of the number of legs in the module.

influence of increasing leg number. Also, in order to compare the importance of including surface to surface radiation, the efficiency of the 2 × 2 and 4 × 4 modules are compared to that of a 2 × 2 module, where all surfaces are assumed to radiate only to the ambient. The efficiency as function of leg separation distance is shown in Fig. 5. As can be seen from the figure, the efficiency of the 2 × 2 and 4 × 4 modules are comparable, with the largest difference being less than 0.2% efficiency. This means that the heat loss computed for the 2 × 2 model can be considered a good approximation of an $n \times n$ system. The difference between including surface to surface and only surface to ambient radiation is also seen to be small, on the order of 0.35% efficiency. This means that the computationally much faster surface to ambient method can be used to estimate the radiative heat loss, at least for the temperatures considered here.

7. Heat losses by convection

Heat loss by convection have been considered previously in the literature for a TEG, by specifying a heat transfer coefficient and not by modelling the actual fluid flow [13−16,18,19]. This approach is a simplification of the true physical problem, in which the heat transfer coefficient must depend on the position on the surface of the leg(s). Here we consider the losses due to natural convection inside a closed and sealed module, filled with air. The module is assumed filled with atmospheric air at atmospheric pressure, with temperature dependent properties, thus the flow is assumed to be compressible. The air is considered transparent to radiation. Transport of heat can thus occur both by radiation between surfaces (of different temperature), conduction through the air and convection. The flow of air is assumed to be laminar.

The hot and cold surfaces of the TEG will establish a gradient in density, which can lead to convective cells. The balance of forces is between the gravitational force on the gradient in density as opposed to the viscous damping force in the fluid. This balance is expressed by the non-dimensional Rayleigh number, Ra_L, defined as

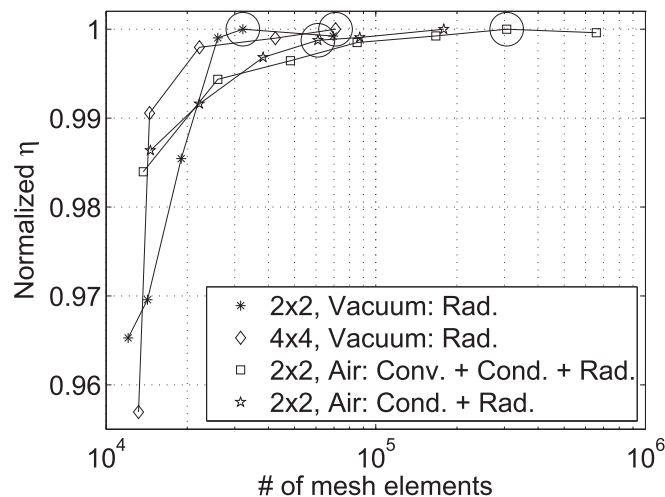$$Ra_L = \frac{g\beta}{\nu\alpha}(T_b - T_t)L^3 \qquad (12)$$

Fig. 3. The normalized efficiency as function of the number of mesh elements of the finite element mesh for some of the different heat loss mechanisms and different number of legs considered. The chosen mesh resolutions have been indicated for the different cases with a circle.
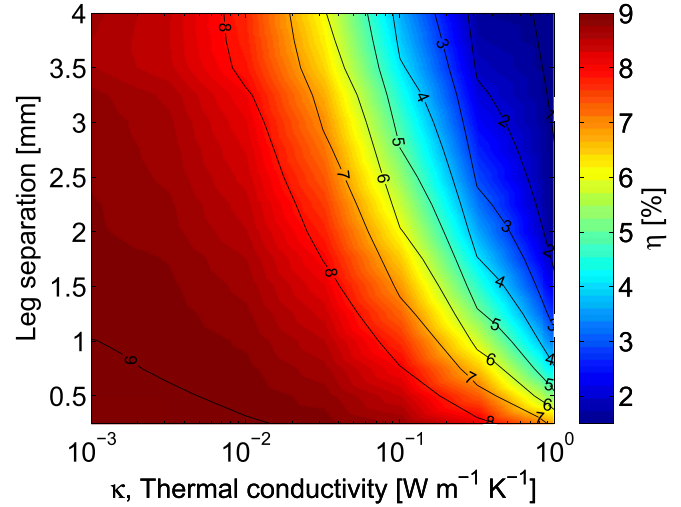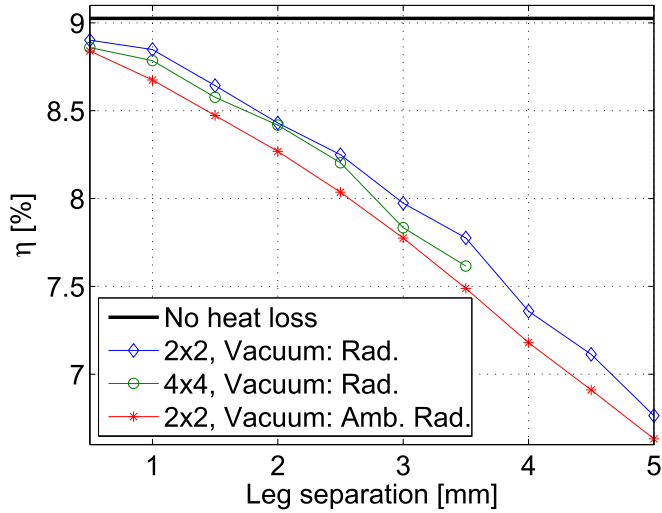
Fig. 5. The efficiency, η, a function of the leg separation distance for a 2×2 and 4×4 module including surface to surface radiation and for a 2×2 module including only surface to ambient radiation. Due to computational resources, only leg separations up to 3.5 mm are considered for the 4×4 module.

where g is the acceleration due to gravity, ν is the kinematic viscosity, α is the thermal diffusivity, β is the thermal expansion coefficient, T_b and T_t is the temperature of the bottom and top plates, respectively, and L is the height of the container.

The critical Rayleigh number depends on the boundary conditions of the system. For the rigid–rigid boundary system of the TEG module, the critical Rayleigh number depends on whether there is vertical velocity symmetry with respect to the mid plane or vertical velocity antisymmetry. The former mode has one row of cells along the vertical while the latter has two rows of cells. The critical Rayleigh numbers are 1707 and 17610 for the two cases, respectively.

For the TEG module, placed with the cold side on top and the hot side on the bottom, the Rayleigh number is on the order of 10–30 for the temperature range and size of module considered here. This means that no convection cells will develop inside the TEG. However, a convective flow can be established inside the TEG if the TEG
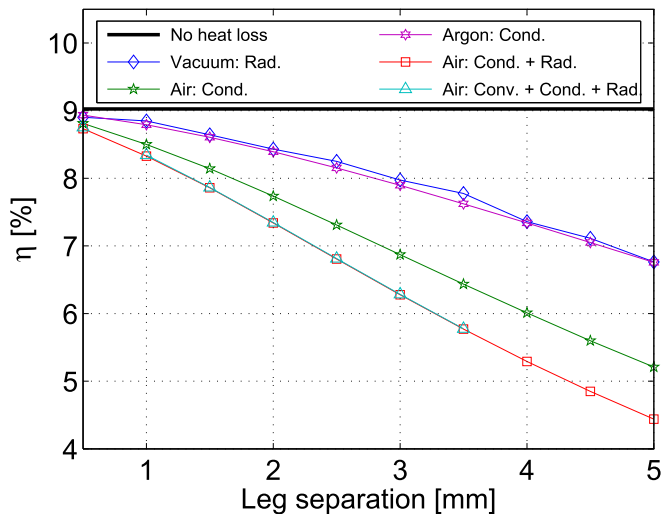

Fig. 6. The efficiency, η, as function of leg separation for the different heat loss cases. Due to computational resources, only leg separations up to 3.5 mm are considered for the convective heat loss case.
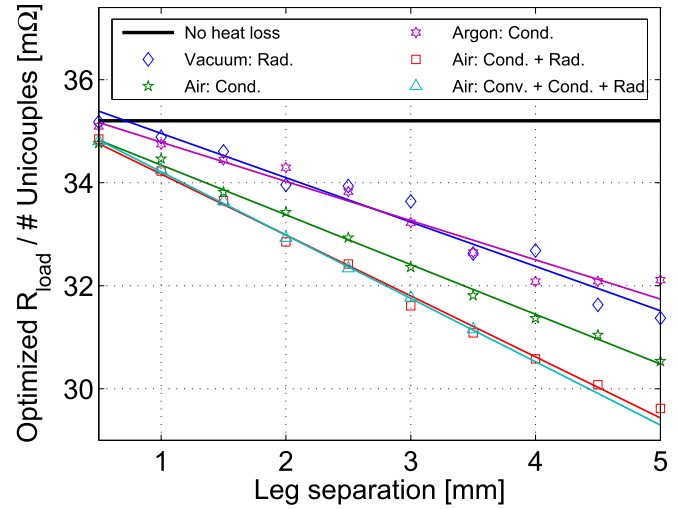

Fig. 7. The optimized load resistance per unicouple as function of leg separation for the same systems as considered in Fig. 6. The lines are straight lines fitted to the data.

is placed such that the hot and cold sides are vertical. In this configuration the air will be heated as it raises along the hot vertical surface and cooled as is falls along the cold vertical surface, allowing a convective flow to be established. This configuration means that the individual air currents are in maximal contact with the heating and cooling surfaces, resulting in the largest convection possible. The efficiency of this configuration will be examined below.

8. Comparing the heat loss mechanisms

We now turn to studying the efficiency as function of leg separation for a combination of the different heat loss mechanisms described above. We consider the efficiency as function of the leg separation for the following cases

- Radiation losses for evacuated module.
- Conduction losses for a module filled with opaque still air ($\kappa = 0.035$ W m^{-1} K^{-1}) or still argon ($\kappa = 0.016$ W m^{-1} K^{-1}).
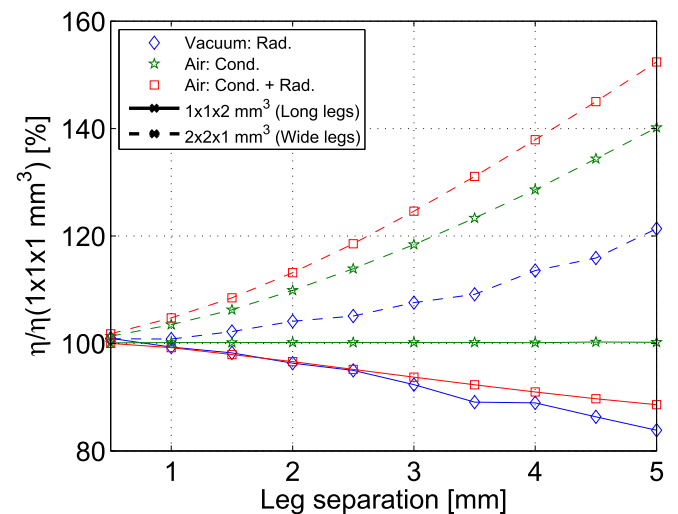

Fig. 8. The efficiency, η, as function of leg separation for the different heat loss cases and for different leg dimensions normalized with the $1 \times 1 \times 1$ mm^3 system. The argon case considered in Fig. 6 is not shown, but results are in trend similar to the case of air.
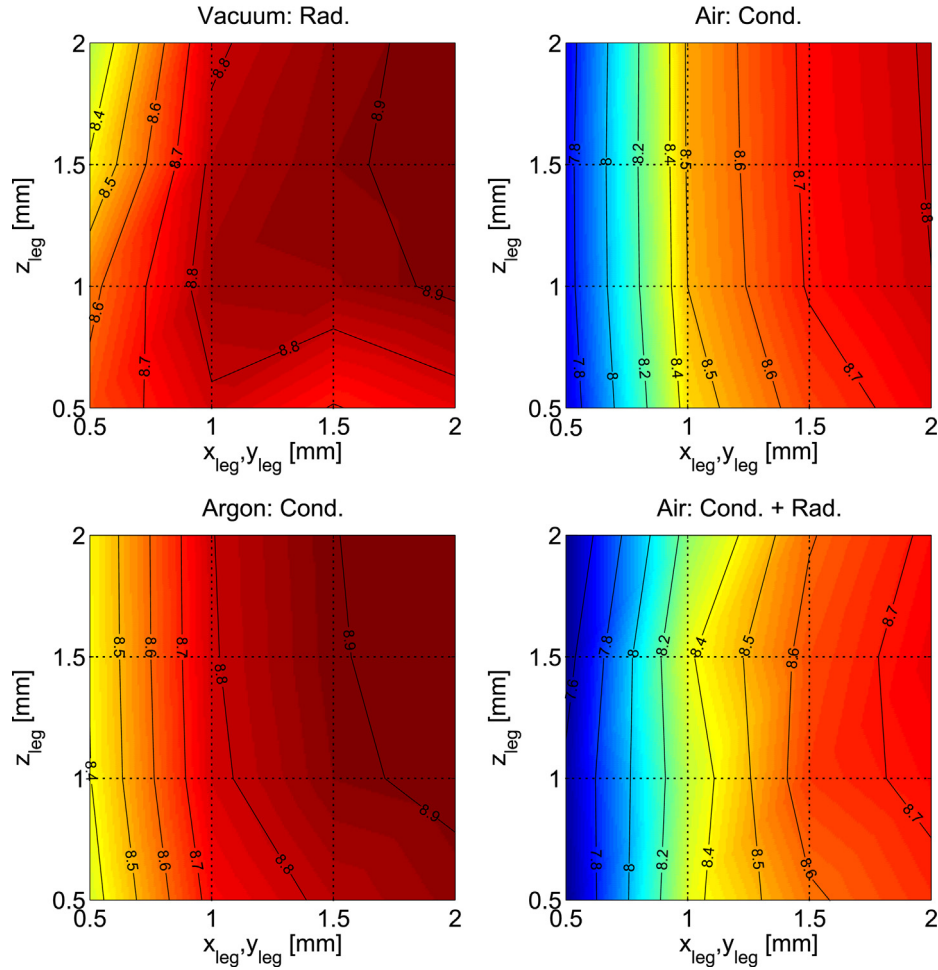
Fig. 9. The efficiency, η, as function of leg dimensions in the $x_{leg} = y_{leg}$ and z_{leg} dimensions, respectively, for a leg separation value of 1 mm, i.e. regardless of the dimensions of the legs there is always 1 mm between the legs. The colour scale is the same for the different heat loss mechanisms. The results are interpolated based on values calculated from 0.5 mm to 2 mm in steps of 0.5 mm. The radiation in vacuum case has a slight numerical variation in the value for the efficiency. (For interpretation of the references to colour in this figure legend, the reader is referred to the web version of this article.)

- Conduction and radiative losses for a module filled with still transparent air.
- Convection, conductive and radiative losses for a vertical module filled with transparent air.

For all these cases the efficiency as a function of leg separation is shown in Fig. 6 for the optimal load resistance. The largest heat loss occurs for the combined case of conduction and radiation. Convection is seen to result in no additional heat loss, even though a nice circular flow can be established inside the TEG, as shown in Fig. 2. The flow velocity is a few mm/s, which, for a module of this size, results in negligible convective heat transfer. The convection results were calculated for a 2x2 module, but convective losses can be expected to be equally negligible for modules with a larger number of legs. Interestingly, the efficiency as function of leg separation is almost the same for a module filled with opaque argon and an evacuated module with only radiation losses. The conclusion is that an efficient module can be designed either with a filled solid insulator or by evacuating the module completely. At higher temperature, radiation losses will increase strongly, as these are proportional to T^4, which means that it is critical to include these in TEG module modelling.

It is also of interest to consider the optimal load resistance for the different heat loss cases. As previously mentioned, the optimal

resistance has been determined for every heat loss mechanism and for all the parameters considered in this study. The resistance varies with leg separation, and thereby heat loss, in a systematic way, decreasing as the leg separation increases. This can be seen in Fig. 7. It is numerically difficult to exactly determine the optimal load resistance, as the efficiency is a shallow function of the load resistance near the optimum value. This results in a small variance in the optimal determined resistances shown in the figure. However, it seems clear that the decrease in load resistance is linear with the leg separation. The reason for this decrease is that as the heat losses increase, it becomes beneficial to operate the TEG at maximum power, rather than at maximum efficiency. Therefore the resistance will go towards the resistance for optimal power, which for the geometry considered above is at 25.6 mΩ per unicouple.

9. Heat loss for different leg dimensions

To determine the heat loss as function of the dimensions of the legs, the efficiency has been computed for modules with wide legs with leg cross-sectional areas, (x_{leg}, y_{leg}), of 2 mm × 2 mm and a leg length, z_{leg}, of 1 mm, and for long legs with leg cross-sectional area of 1 mm × 1 mm and a leg length of 2 mm. As previously, the size of the n- and p-leg is equal. These are wider and longer legs,

respectively, than the 1 mm × 1 mm × 1 mm legs considered above. The normalized efficiency as function of leg separation distance is shown in Fig. 8 for the different heat loss cases. When only conduction is considered, increasing the leg length and with a fixed cross-sectional area the efficiency remains constant. This is expected due to the adiabatic boundary conditions, as well as the almost linear temperature profile along the legs, which means that heat loss from the leg to the air is negligible. In the radiation case, longer legs lead to larger heat loss, as the legs have a larger surface from which to radiate heat to the cold plate. The wide legs are seen to substantially increase the efficiency for both the radiative and conductive heat loss cases. This is due to a smaller surface to cross-sectional area ratio, which leads to lower heat loss compared to the amount of heat flowing through the leg. The use of wider legs is seen to be increasingly beneficial at larger leg separations, due to the increased cross-sectional area of the legs compared to that of the top plate.

The decrease in efficiency for longer or larger legs can be understood by noting that heat losses have the least effect on the efficiency if the majority of the heat flows through the legs and only a minor fraction bypasses the active material via the heat loss mechanisms. Scaling the absolute leg size with a factor x, increases the conduction flow through the legs linearly as the cross-sectional area increases quadratically, but the length increases linearly. However, the leg surface area where the heat losses occur scales quadratically. Thus, when up-scaling the legs, heat losses becomes more dominant. Instead, shorter legs and large cross-sectional areas are optimal in reducing heat losses.

The heat loss as function of the leg cross-sectional area, $x_{\text{leg}} = y_{\text{leg}}$, and leg length, z_{leg}, has also been considered for a fixed leg separation of 1 mm. Fig. 9 show the efficiencies of the module for different legs dimensions and heat losses based on calculated leg values of 0.5 mm–2 mm in steps of 0.5 mm. As seen in Fig. 9, increasing the legs cross-sectional area, $(x_{\text{leg}}, y_{\text{leg}})$ increases the efficiency of the module while changing the length of the legs only decreases the efficiency in the case of radiative heat loss. This is as observed in Fig. 8. Note that, as previously mentioned, had the legs had different temperature profiles due to different material properties, the legs will start to cross-talk thermally at small separations in the conduction case also. The ideal way to construct a TEG module with minimal heat losses is thus to use a good insulating material between the legs, properly seal the module and using small and wide, closely spaced legs.

10. Conclusion

A three dimensional numerical finite element model of a thermoelectric generator consisting of p- and n-leg bismuth telluride has been developed. The model was compared with a one dimensional numerical model for the case of no heat losses and the results were shown to be identical. Next, different heat loss mechanisms were investigated for a closed module. Both surface to surface radiative heat transfer, conductive and convective heat transfer were considered, and both separately and simultaneously. First, the influence of surface to surface radiation was shown to be small for the hot side temperature of 523.15 K considered here and using the simpler surface to ambient radiation is sufficient. Second, for conductive heat transfer the efficiency as function of thermal conductivity and unicouple separation was determined. Third, heat losses due to convection inside the module were shown to be negligible for the module size considered here. Comparing the heat loss mechanisms, it was shown that for an insulator with properties similar to argon, the efficiency is comparable to radiative heat losses. The efficiency was significantly lower for combined radiative and conduction heat transfer. Investigating the dimensions of the

legs showed that the ideal way to construct a TEG module with minimal heat losses is to either use a good insulating material between the legs or evacuate the module completely, and use small and wide legs closely spaced.

References

[1] M.S. El-Genk, H.H. Saber, T. Caillat, J. Sakamoto, Tests results and performance comparisons of coated and un-coated skutterudite based segmented unicouples, Energ. Convers. Manag. 47 (2) (2006) 174–200.
[2] L.T. Hung, N.V. Nong, L. Han, R. Bjørk, P.H. Ngan, T.C. Holgate, S. Linderoth, B. Balke, G.J. Snyder, N. Pryds, Segmented thermoelectric oxide-based module, Energy (2014) submitted for publication.
[3] A. Muto, D. Kraemer, Q. Hao, Z.F. Ren, G. Chen, Thermoelectric properties and efficiency measurements under large temperature differences, Rev. Sci. Instrum. 80 (9) (2009) 093901.
[4] F. Meng, L. Chen, F. Sun, A numerical model and comparative investigation of a thermoelectric generator with multi-irreversibilities, Energy 36 (5) (2011) 3513–3522.
[5] H. Kim, O.J. Kim, K.H. Lee, P.W. Heo, B.S. Choi, Finite element analysis of a thin-film thermoelectric module for thermal management in micro electronics, in: PowerMEMS 2009, Washington DC, USA, December 1–4, 2009, p. 281.
[6] D. Ebling, K. Bartholom, M. Bartel, M. Jgle, Module geometry and contact resistance of thermoelectric generators analyzed by multiphysics simulation, J. Electron. Mater. 39 (9) (2010) 1376–1380.
[7] B. Jang, S. Han, J.-Y. Kim, Optimal design for micro-thermoelectric generators using finite element analysis, Microelectron. Eng. 88 (5) (2011) 775–778.
[8] T. Seetawan, U. Seetawan, A. Ratchasin, S. Srichai, K. Singsoog, W. Namhongsa, C. Ruttanapun, S. Siridejachai, Analysis of thermoelectric generator by finite element method, Proc. Eng. 32 (2012) 1006–1011.
[9] X.D. Wang, X.X. Zhang, J.H. Meng, Transient modeling and dynamic characteristics of thermoelectric cooler, Appl. Energy 108 (2013) 340–348.
[10] Y.-X. Huang, X.-D. Wang, C.-H. Cheng, D.T.-W. Lin, Geometry optimization of thermoelectric coolers using simplified conjugate-gradient method, Energy 59 (2013) 689.
[11] X.D. Wang, X.X. Zhang, J.H. Meng, Dynamic response characteristics of thermoelectric generator predicted by a three-dimensional heat-electricity coupled model, J. Power Sources 245 (2014) 262–269.
[12] R. Harris, T.-P. Shih, T. Hogan, H. Schock, T.-P. Shih, Heat transfer and electric current flow in a thermoelectric couple, in: Collection of Technical Papers — 44th AIAA Aerospace Sciences Meeting, vol. 10, 2006, pp. 6855–6869.
[13] M. Chen, L.A. Rosendahl, T. Condra, A three-dimensional numerical model of thermoelectric generators in fluid power systems, Int. J. Heat Mass Transfer 54 (2011) 345–355.
[14] B. Reddy, M. Barry, J. Li, Mathematical modeling and numerical characterization of composite thermoelectric devices, Int. J. Therm. Sci. 67 (2013) 53.
[15] A. Bauknecht, T. Steinert, C. Spengler, G. Suck, Analysis of annular thermoelectric couples with nonuniform temperature distribution by means of 3-d multiphysics simulation, J. Electron. Mater. 42 (7) (2013) 1641–1646.
[16] T. Yang, J. Xiao, P. Li, P. Zhai, Q. Zhang, Simulation and optimization for system integration of a solar thermoelectric device, J. Electron. Mater. 40 (5) (2011) 967–973.
[17] X.-D. Wang, Y.-X. Huang, C.-H. Cheng, D.T.W. Lin, C.-H. Kang, A three-dimensional numerical modeling of thermoelectric device with consideration of coupling of temperature field and electric potential field, Energy 47 (1) (2012) 488–497.
[18] H.H. Saber, M.S. El-Genk, A three-dimensional, performance model of segmented thermoelectric converters, AIP Conf. Proc. 608 (1) (2002) 998.
[19] P. Ziolkowski, P. Poinas, J. Leszczynski, G. Karpinski, E. Mller, Estimation of thermoelectric generator performance by finite element modeling, J. Electron. Mater. 39 (9) (2010) 1934–1943.
[20] Tegnergatan 23, SE-111 40 Stockholm, Sweden, Comsol Multiphysics, A, 2013.
[21] Y. Yang, S.H. Xie, F.Y. Ma, J.Y. Li, On the effective thermoelectric properties of layered heterogeneous medium, J. Appl. Phys. 111 (1) (2012) 013510.
[22] Y. Ma, Q. Hao, B. Poudel, Y. Lan, B. Yu, D. Wang, G. Chen, Z. Ren, Enhanced thermoelectric figure-of-merit in p-type nanostructured bismuth antimony tellurium alloys made from elemental chunks, Nano Lett. 8 (8) (2008) 2580–2584.
[23] C. Kim, D.H. Kim, H. Kim, J.S. Chung, Significant enhancement in the thermoelectric performance of a bismuth telluride nanocompound through brief fabrication procedures, ACS Appl. Mater. Interfaces 4 (6) (2012) 2949–2954.
[24] G.J. Snyder, T.S. Ursell, Thermoelectric efficiency and compatibility, Phys. Rev. Lett. 91 (14) (2003) 148301.

[25] D.M. Rowe (Ed.), Thermoelectrics Handbook — Macro to Nano, Taylor and Francis Group, LLC, 2006.

[26] G. Fraisse, J. Ramousse, D. Sgorlon, C. Goupil, Comparison of different modeling approaches for thermoelectric elements, Energ. Convers. Manag. 65 (2013) 351—356.

[27] Marlow Industries, Inc, 2013, Private communication.

[28] E. Lemmon, R. Jacobsen, S. Penoncello, D. Friend, Thermodynamic properties of air and mixtures of nitrogen, argon, and oxygen from 60 to 2000 K at pressures to 2000 MPa, J. Phys. Chem. Ref. Data 29 (3) (2000).

[29] The latest version of Comsol, 4.4, has built-in support of thermoelectric materials. The implementation discussed here is equivalent to this implementation.